Optical and Quantum Electronics (2021) 53:149
https://doi.org/10.1007/s11082-021-02798-y

An ultra-fast optical analog-to-digital converter using nonlinear X-shaped photonic crystal ring resonators

Saleh Naghizade[1] · Hamed Saghaei[2]

Received: 28 December 2020 / Accepted: 20 February 2021 / Published online: 28 February 2021

Abstract
This paper reports a new optical analog-to-digital converter (OADC) design based on nonlinear X-shaped photonic crystal ring resonators (X-PCRRs). The dielectric rods made of silicon and nonlinear rods composed of doped glass are used to form X-PCRRs. The proposed structure consists of a nonlinear three-channel demultiplexer and an optical encoder. The nonlinear demultiplexer converts the continuous input signal into three quantized discrete levels, and the optical encoder generates two-bit binary codes depending on the output channel number of the demultiplexer. Two well-known plane wave expansion and finite difference time domain methods are applied to study and analyze the photonic band structure and light propagation inside the PhC-based structure, respectively. The wide TM photonic band gap of the fundamental PhC covers the second window of telecommunication in the C-band. Our calculations reveal that the proposed OADC has a maximum response time of about 4 ps and a sampling rate of 125 GS/s that is much faster than the designed ADC in previous studies. The proposed ADC also has a total footprint of 1785 μm^2 with a minimum leakage loss.

Keywords Analog-to-digital converter · Photonic crystal · Nonlinear ring resonator · Optical Kerr effect · Demultiplexer · Optical encoder

1 Introduction

Photonic crystal fibers (PCFs) and photonic crystal slabs (PCSs) are appropriate tools for implementing all-optical telecommunication systems and networks (Sinha and Rawal 2008). These structures are periodic arrays of dielectric materials (Rahmani and Mehdizadeh 2018; Saghaei et al. 2017; Sharifi et al. 2016). They have many applications in the design of logic gates (Andalib and Granpayeh 2009; Hussein et al. 2018; Moradi et al. 2019; Younis et al. 2014), optical filters (Alipour-Banaei et al. 2014; Foroughifar et al. 2021; Guo et al. 2019; Naghizade and Saghaei 2020a; Rakhshani and Mansouri-Birjandi

✉ Hamed Saghaei
h.saghaei@iaushk.ac.ir

[1] Young Researchers and Elite Club, Tabriz Branch, Islamic Azad University, Tabriz, Iran

[2] Department of Electrical Engineering, Shahrekord Branch, Islamic Azad University, Shahrekord, Iran

2013), encoders and decoders (Moniem 2016; Monisha et al. 2018; Mostafa and El-Rabaie 2019; Naghizade and Khoshsima 2018; Parandin 2019; Parandin et al. 2018; Rajasekar et al. 2020; Yang et al. 2017; Naghizade and Saghaei 2020b), comparators (Fakouri-Farid and Andalib 2018; Jile 2020), adders and subtractors (Hosseinzadeh Sani et al. 2020a; Moradi et al. 2018; Moradi 2019), registers (Martinez-Dorantes et al. 2017; Pahari and Guchhait 2012), optical fibers (Aliee et al. 2020; Diouf et al. 2017; Ghanbari et al. 2018, 2017; Saghaei 2017; Saghaei et al. 2016a, 2016b, 2015), demultiplexers (Mehdizadeh and Soroosh 2016; Saghaei et al. 2011; Saghaei and Seyfe 2008; Talebzadeh et al. 2017; Wen et al. 2012), sensors (Alden Mostaan and Saghaei 2021; Hosseinzadeh Sani et al. 2020b; Kowsari and Saghaei 2018; Nasirifar et al. 2019; Tabrizi et al. 2021; Tavakoli et al. 2019), PhC fibers (Ebnali-Heidari et al. 2014; Raei et al. 2018; Saghaei 2018; Saghaei and Ghanbari 2017; Saghaei and Van 2019), switches (Alipour-Banaei et al. 2015; Chen et al. 2006; Danaie and Kaatuzian 2011; Mehdizadeh et al. 2017a), interferometers (Danaee et al. 2019; Gu et al. 2007; Saghaei et al. 2019), and memories (Alexoudi et al. 2020; Kuramochi et al. 2014; Uda et al. 2018), as well as all-optical clocked sequential circuits including flip-flops (Kumar et al. 2010; Sethi and Roy 2014), synchronous and asynchronous counters (Kaur and Kaler 2014; Poustie et al. 2000). Another important application is the use of photonic crystals in the optical analog-to-digital converter. An OADC generates binary code from the light intensity of the input signal. Researchers have shown that the optical behavior of PhC-based structures depends significantly on the refractive index. However, we know that due to the optical Kerr effect, the refractive index of the dielectric material depends on the intensity of the incoming light. Overall, this means that PhC-based structures can be used in the design of OADCs because their optical behavior can be controlled by light intensity. Miao et al. (2006) reported a two-bit OADC by the use of cascaded beam-splitters. Youssefi et al. (2012) applied a nonlinear optical Kerr effect on 2D photonic crystals. They designed a two-bit OADC including two drop filters with a selective reflector. It has a maximum speed of 45 GS/s in an area of 252 μm^2. Sani et al. (2020) proposed a two-bit OADC using nonlinear ring resonators with AlGaAs dielectric rods. This converter has a sampling rate of 220 GS/s and an area of about 778 μm^2. Fasihi (2014) designed another two-bit OADC using a PhC structure based on cascading splitters. It can be used to form the design of two- and three-bit OADCs in the PhC structure. Tavousi and Mansouri-Birjandi (2018) has recently proposed a successive approximation-like four-bit full OADC using photonic crystal ring resonators (PCRRs) with nonlinear rods. Jafari et al. (2018) also reported a design of an OADC based on the optical Kerr effect in the PhC structure, which performs properly at the C-band (1550 nm). A cavity was also designed using nonlinear materials in order to convert the optical analog signals into digital numbers with a speed of 1 TS/s. The best results are achieved in this study; unfortunately, they were examined based on the Kerr effect's unreal value. As a result, no material could be found with this highly nonlinear refractive index.

The present study will address all mentioned issues in previous studies and propose high-speed OADC based on nonlinear PCRRs. We propose an OADC for generating standard binary codes from the input optical analog signal. The proposed structure consists of two main parts: a nonlinear demultiplexer for performing the quantization task, and an optical coder for generating two-bit standard codes from the quantized levels coming from the nonlinear demultiplexer. In order to perform the required simulations and calculations, the plane-wave expansion and finite-difference time-domain (FDTD) methods are used. In order to take advantage of the nonlinear Kerr effect, we included the nonlinear coefficient in the numerical method and used the nonlinear FDTD method for simulating the proposed structures. The rest of the paper is organized as follows: In Sect. 2, the design procedure of the proposed OADC is presented, in Sect. 3 the numerical results are discussed, and finally, in Sect. 4, the paper is closed with the conclusion.

2 Physical structure and analysis

A schematic view of a conventional ADC consisting of a quantizer and an encoder is shown in Fig. 1a. The figure proposes a new design of two-bit OADC based on nonlinear PCRRs. The sampling and quantization are performed via a nonlinear demultiplexer and coded via a binary encoder. The nonlinear demultiplexer quantizes the optical input signal into four discrete levels depending on the signal intensity, and the coder assigns a two-bit binary number to every level. The fundamental PhC structure used for designing the OAC has a square lattice of dielectric rods in the air bed. The refractive index and radius of the dielectric rods are assumed to be n = 3.46 and R = 0.2 a, respectively, where a is the lattice constant of the structure (i.e., the distance between two centers of adjacent dielectric rods).

2.1 The band diagram

Figure 1b shows the band diagram of the fundamental PhC structure. It has been calculated through the plane wave expansion (PWE) method using the BandSOLVE software. The figure reveals that the fundamental structure has two photonic band-gap (PBG) regions in TM mode (shown in blue) and one PBG in TE mode (shown in red).

The first PBG region in TM mode is in the normalized frequency range of $0.28 < a/\lambda < 0.45$, and by choosing a = 600 nm, the PBG will be in the wavelength range of 1333 nm $< \lambda <$ 2142 nm. Considering the PBG region, this fundamental PhC is suitable for designing optical devices at the third communication window in TM mode.

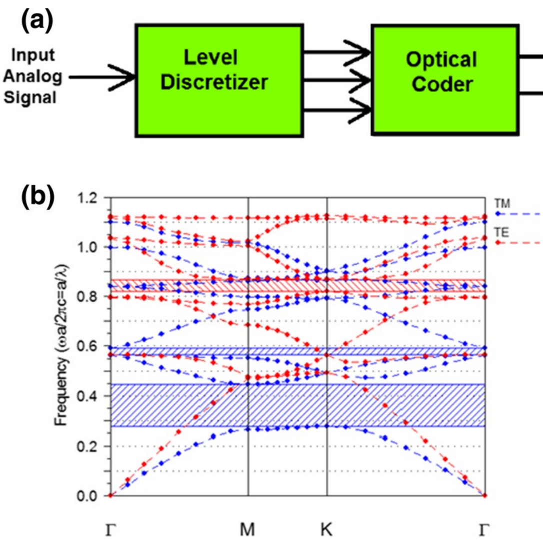

Fig. 1 Illustration of **a** The block diagram of a conventional ADC and **b** The photonic band diagram representation of the fundamental TE- and TM-like modes in PhC

In order to realize the proposed OADC, we need to carry out two main steps. First, we should sample and quantize the incoming light and then produce two-bit binary codes corresponding to these levels.

2.2 Nonlinear demultiplexer

A nonlinear demultiplexer is used as the quantizer of the proposed ADC. This part converts the continuous input signal into three quantized discrete levels.

This quantization is based on the optical intensity of the input signal, and therefore the demultiplexer should be designed to direct the input light to the desired output depending on its intensity. To achieve this goal, we used three nonlinear PCRRs for the basic demultiplexer design. As shown in Fig. 2a, three hexagonal structures were used as the main part (called core) of the PCRRs. In order to take advantage of the nonlinear optical Kerr effect, we placed a set of X-shaped dielectric rods inside the core. These rods were made of doped glass whose linear refractive index and nonlinear optical Kerr coefficient are 1.4 and 10^{-14} m^2/W, respectively. They are shown in pink in Fig. 2b. The optical behavior of the demultiplexer can be controlled using nonlinear rods in each of the resonators. The resonant wavelength of the PCRR depends on the refractive index of the core rods. Due to the optical Kerr effect of nonlinear rods, the refractive index of nonlinear rods increases by increasing the light intensity that it changes the resonant wavelength.

The frequency response of the proposed demultiplexer is shown in Fig. 3 for the input pulse width of 8 ps. As seen, the demultiplexer has three resonant modes at1552nm, 1562 nm, and 1571 nm, respectively. The demultiplexer outputs in terms of time for different input optical intensities (I_{in}) are shown in Fig. 4. The amount of normalized power at O1, O2, and O3 are shown in green, red, and blue curves, respectively.

In Fig. 5, the optical signals' distribution inside the demultiplexer is shown for different values of input optical intensity. According to Fig. 4, for $0 < I_{in} < 0.5I_0$,(where $I_0 = 1$ W/μm^2), none of the demultiplexer ports will be ON, but when the optical intensity of the input signal is at $0.5I_0 < I_{in} < I_0$, $I_0 < I_{in} < 1.5I_0$, and $1.5I_0 < I_{in} < 2I_0$, O3, O1, and O2 will be ON, respectively. It is due to the nonlinear optical Kerr effect and refractive index dependency of the ring resonators' resonant mode. When the optical intensity is less than $0.5I_0$, none of the resonant rings can couple the optical beam to their corresponding output ports because the optical signal's central wavelength is different from the resonant mode of the rings.

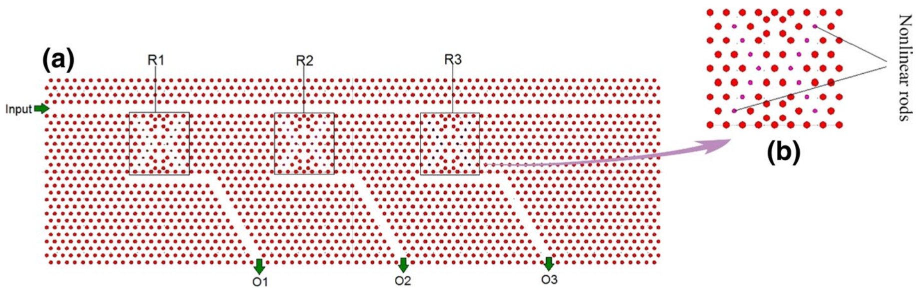

Fig. 2 **a** The proposed three-channel demultiplexer and the **b** the nonlinear PCRR

Fig. 3 Transmission spectra at the outputs O1, O2, and O3 of the proposed demultiplexer

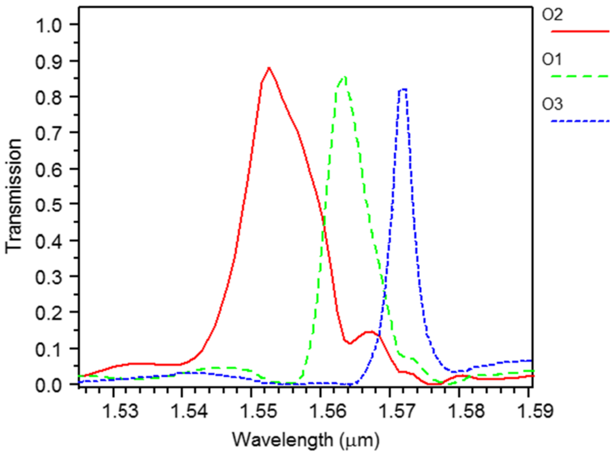

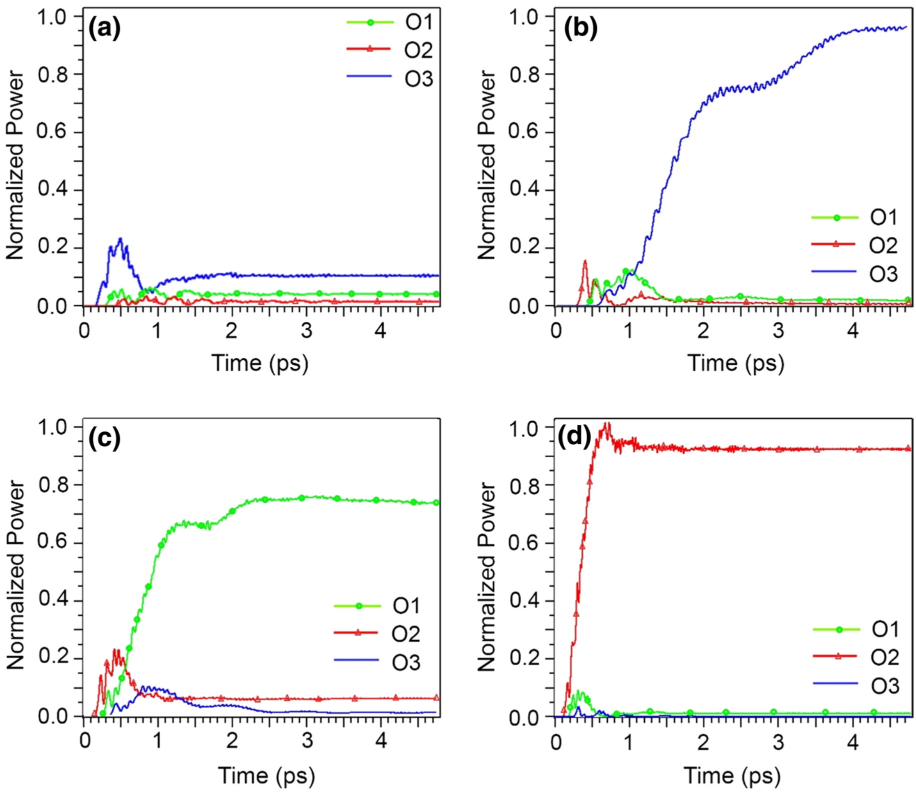

Fig. 4 The demultiplexer outputs in terms of time for different input optical intensities of **a** $0 < I_{in} < 0.5I_0$, **b** $0.5I_0 < I_{in} < I_0$, **c** $I_0 < I_{in} < 1.5\ I_0$, and **d** $1.5\ I_0 < I_{in} < 2I_0$

Figure 4a shows that the normalized power for all the output ports is less than 10%. By increasing the optical intensity to more than $0.5I_0$ and less than I_0, the third ring's resonant mode will coincide with the central wavelength of the input signal. Therefore, as shown in

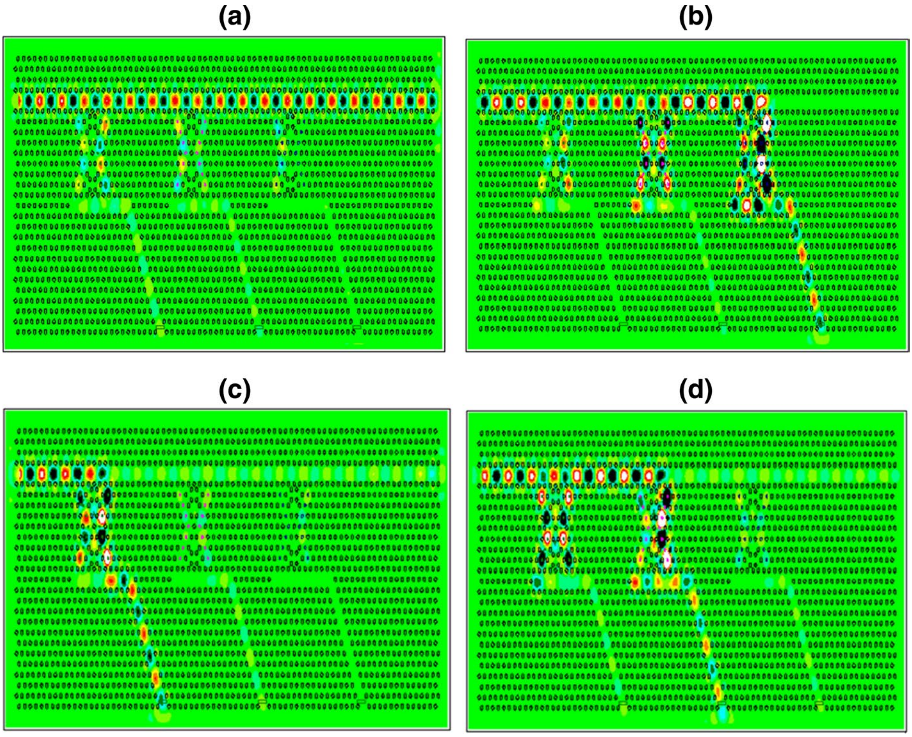

Fig. 5 Optical behavior of the nonlinear demultiplexer for the optical intensities of **a** $0<I_{in}<0.5I_0$, **b** $0.5I_0<I_{in}<I_0$, **c** $I_0<I_{in}<1.5\ I_0$, and **d** $1.5\ I_0<I_{in}<2I_0$

Fig. 4b, the normalized power for O3 is about 95% and for other channels is less than 2%. If we increase the optical intensity to $I_0<I_{in}<1.5I_0$, the normalized power for O1 is about 75% and for other channels is less than 5% (See Fig. 4c). Finally, when the optical intensity is in the range of $1.5I_0<I_{in}<2I_0$, the normalized power for O2 is about 95% and for other channels is less than 2% (See Fig. 4d).

2.3 Optical encoder

Once discrete signal levels are generated, assigning a two-bit binary code to each level is necessary. It is performed using an optical encoder proposed in this study and shown in Fig. 6. As seen, it consists of three input ports, two waveguides created by removing two rows of dielectric rods, two X-shaped ring resonators, a Y-branch power splitter, and two output ports. As seen, the encoder input ports are I_1, I_2, and I_3, and its output ports are O1 and O2. In this structure, the R1 ring can couple the optical waves from WG1 to WG2, and R2 couples the optical waves from WG3 to WG4. Note that it is impossible to couple waves from WG2 to WG1 and WG4 to WG3 using R1 and R2, respectively, because the light intensity in WG2 and WG4 waveguides does not correspond to the intensity required for coupling in resonators. As we mentioned earlier, R1 and R2 are nonlinear X-shaped ring resonators; therefore, their optical behavior and resonant modes depend on the optical intensity propagating inside the waveguides.

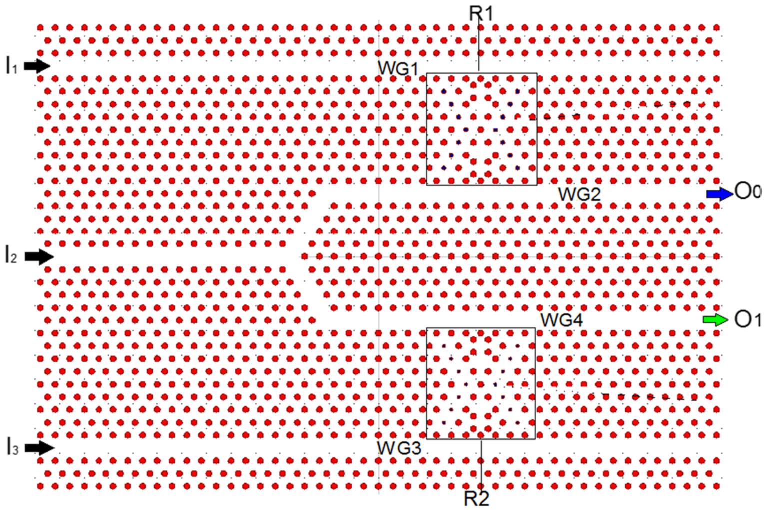

Fig. 6 The schematic view of the designed optical encoder in this study

The encoder's input ports have been connected to the output ports of the nonlinear demultiplexer; therefore, the intensity of incoming light to the encoder is different. As a result, the optical intensities inside WG1 and WG3 are different from the optical intensities propagating inside WG2 and WG4. For the optical intensities coming from I_1 and I_3, inside WG1 and WG3, the resonant mode of R1 and R2 matches the central wavelength of the optical waves, so R1 and R2 will drop optical waves from WG1 and WG3 into WG2 and WG4, respectively. However, for the optical intensities coming from I_2 inside WG2 and WG4, the resonant mode of R1 and R2 does not match the central wavelength of the optical waves. Therefore R1 and R2 cannot drop optical waves from WG2 and WG4 into WG1 and WG3, respectively. The optical behavior of the designed encoder is shown in Fig. 7. As shown in Fig. 7a, when I_1 is ON, considering the optical intensity coming from I_1, the resonant mode of R1 coincides with the optical signal, so R1 will couple the optical signal from WG1 to WG2, and O1 will be ON. When I_2 is ON, the Y-branch splits the light intensity of I_2 into two equal values, and each of these intensities does not match the corresponding resonator coupling mode. Then R1 and R2 cannot couple the optical waves due to low light intensity, so the optical beams travel toward O1 and O2 and turn them ON (See Fig. 7b). When I_3 is ON, considering the optical intensity coming from I_3, the resonant mode of R2 coincides with the input optical signal; thus, R2 will couple the optical signal from WG3 to WG4, and O2 will be ON (See Fig. 7c).

3 The proposed OADC

In order to design an OADC, the nonlinear demultiplexer is connected to the optical encoder.

An 87×57 matrix of triangular-latticed silicon rods forms the base structure of our OADC. All physical parameters of the structure are in accordance with the values stated in the first paragraph of this section. In order to realize the proposed OADC inside the basic PhC structure, we need to create five resonant rings and six waveguides. The schematic

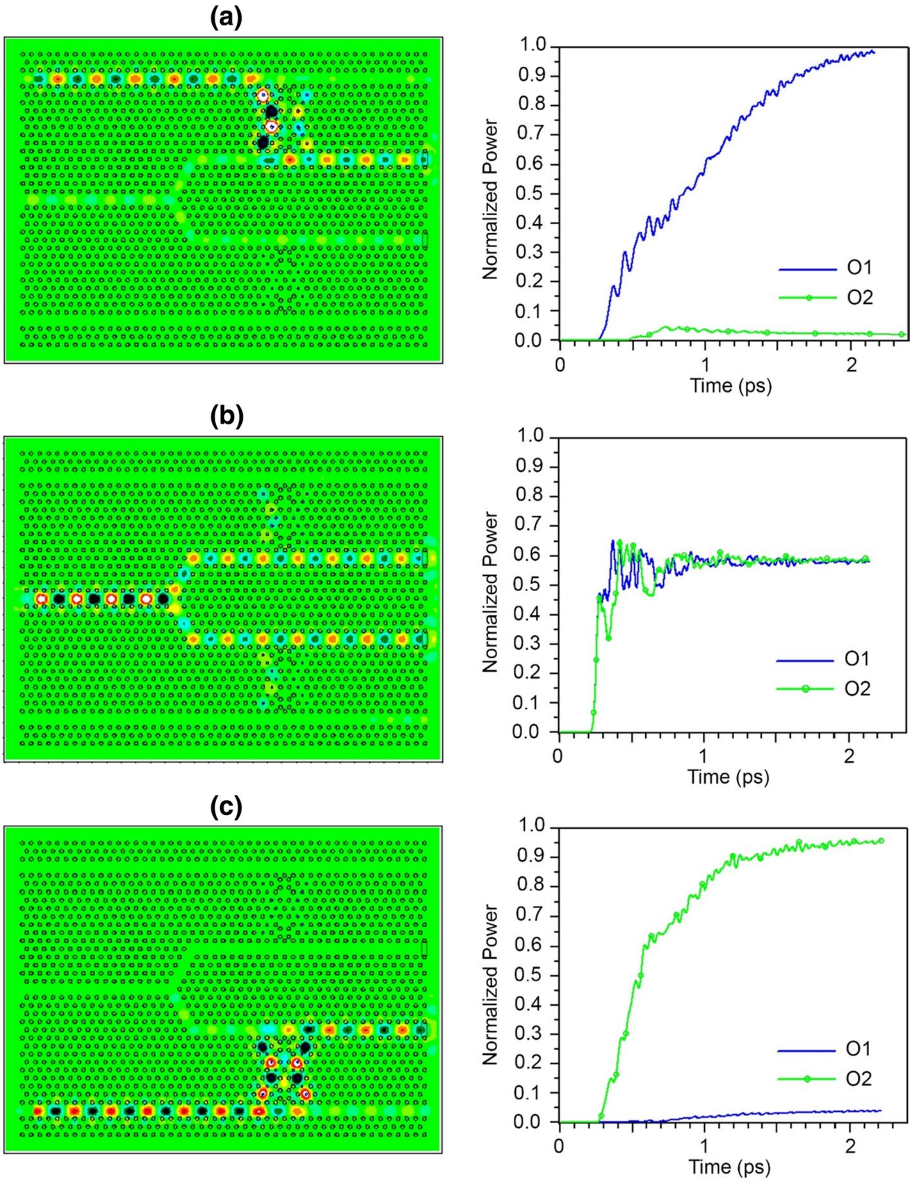

Fig. 7 The optical behavior and output time response of the proposed encoder for three input states of **a** I_1 is active, I_2 and I_3 are inactive, **b** I_2 is active, I_1 and I_3 are inactive, **c** I_3 is active, I_1 and I_2 are inactive

view of the proposed OADC is shown in Fig. 8 where it has one input and two output ports (called O0 and O1). WG1 serves as the input waveguide. The end of WG1 is open in order to prevent back reflection of the optical signals toward the input port. Three X-shaped ring resonators labeled as R1, R2, and R3 perform the optical quantization process. WG2, WG3, and WG4 guide the dropped optical waves through R1, R2, and R3 toward the R4 and R5 resonators, respectively. The optical properties of R1 and R3 are the same as R4

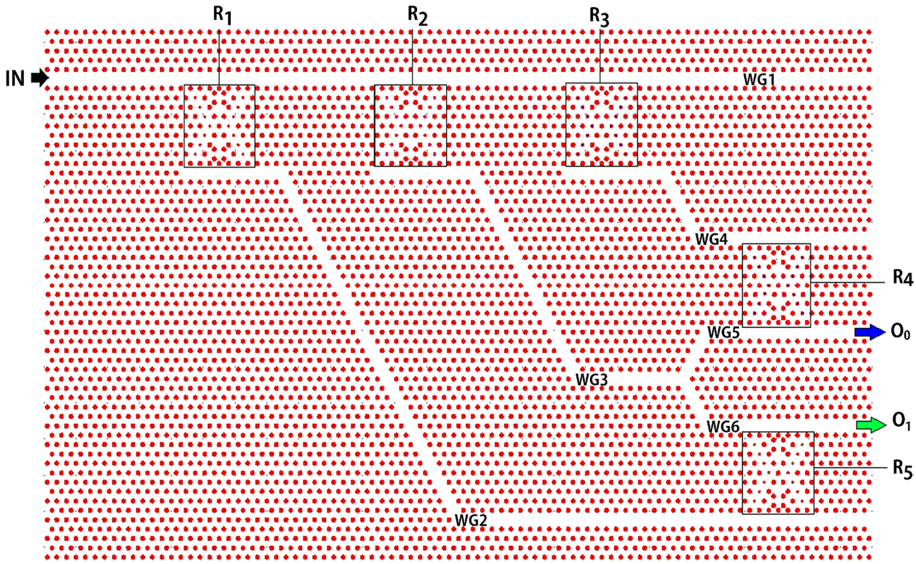

Fig. 8 The schematic view of the proposed two-bit OADC

and R5, respectively. However, the optical properties of R2 are different from R4 and R5. Therefore, R4 can drop the optical waves from WG4 into WG5, but it cannot drop optical waves from WG5 into WG4 due to its low optical intensity. In addition, R5 can drop the optical waves from WG2 into WG6, but it cannot drop optical waves from WG6 into WG2. As discussed in the previous subsection, all the optical ring resonators are nonlinear, which means their optical behavior and resonant modes depend on the optical intensities propagating inside the waveguides. Additionally, it was mentioned that R1, R2, and R3 drop optical waves with different optical intensities. When R1 and R5 have similar optical and structural parameters, they will drop optical waves with the same intensities; therefore, R5 will drop optical waves coming from R1 inside WG2 to WG6.

Similarly, when R3 and R4 have similar optical and structural parameters, they will drop optical waves with the same intensities; therefore, R5 will drop optical waves coming from R3 inside WG4 into WG5. The ends of WG5 and WG6 are connected to the O0 and O1 output ports, respectively. When R2 drops optical waves into WG3, the Y-branch splits the light intensity into two equal values, and each of these intensities does not match the corresponding resonator coupling mode. R4 and R5 cannot couple the optical waves to WG4 and WG5 due to low light intensity. Thus the optical beams travel toward O0 and O1 using WG5 and WG6, respectively.

The optical behavior of the proposed OADC is shown in Fig. 9. For the optical intensity of the input signal in the range of $0<I_{\text{in}}<0.5I_0$ as discussed earlier, due to the mismatch between the resonant mode and the central wavelength of the resonators, none of the resonators would couple the optical beam from the input port to their corresponding output waveguides. Therefore, both of the output ports will be OFF, as shown in Fig. 9a, and the generated logical code will be '00′. Furthermore, Fig. 10a shows that the normalized powers for both output ports are less than 5%. When the optical intensity is about $0.5I_0<I_{\text{in}}<I_0$, R3 will couple the optical beam from WG1 into WG4, and the optical beam will travel toward R4 through WG4. Then R4 drops the optical waves from WG4 into WG5; thus,

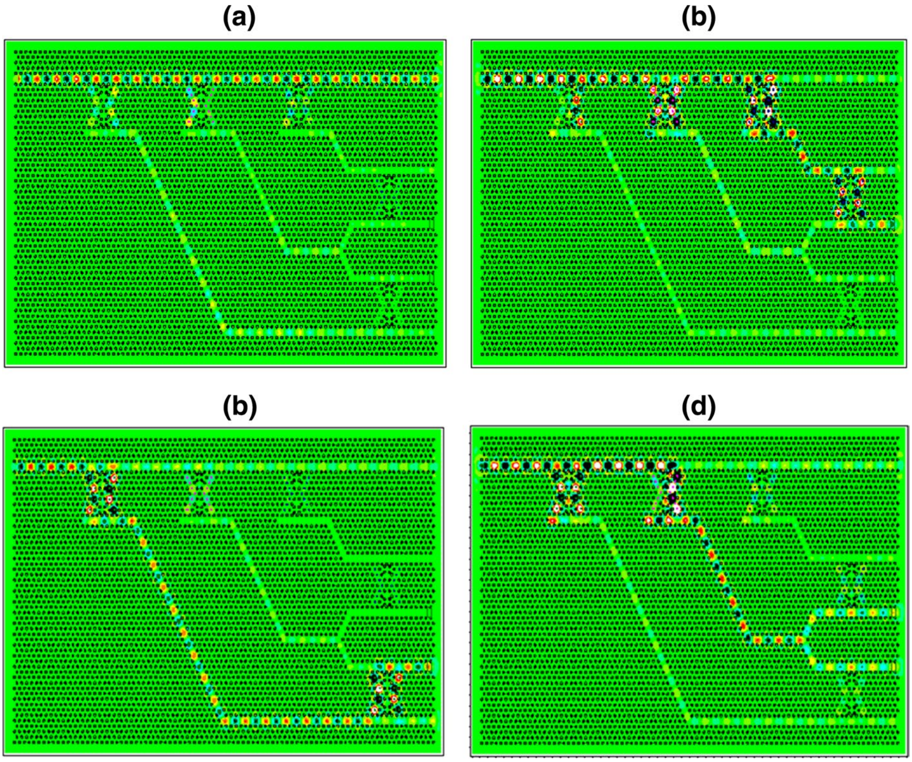

Fig. 9 The optical behavior of the proposed OADC for the optical intensities of **a** $0<I_{in}<0.5I_0$, **b** $0.5I_0<I_{in}<I_0$, **c** $I_0<I_{in}<1.5\ I_0$, and **d** $1.5\ I_0<I_{in}<2I_0$

O0 will be active; however, there is no optical beam in WG5, and the O1 is inactive (See Fig. 9b). Therefore, in this case, the generated binary code is "10." Figure 10b shows that the normalized output powers of O0 and O1 are about 70% and 5%, respectively. In this case, the time required for the normalized power at O0 to reach the steady-state is about 2.5 ps.

For an optical intensity in the range of $I_0<I_{in}<1.5I_0$, R1 will couple the optical beam from WG1 into WG2, and the optical beam will travel toward R5 through WG2, and R5 drops the optical waves from WG2 into WG6, so O1 will be active; however, there is no optical beam in O0 (See Fig. 9d). As a result, when $I_0<I_{in}<1.5I_0$, the generated code will be "01." Figure 10d shows that the normalized output powers of O0 and O1 are about 2% and 95%, respectively. In this case, the steady-state time is about 2.5 ps.

Finally, when the input optical intensity is in the range of $1.5I_0<I_{in}<2I_0$, R2 will couple the optical beam from WG1 into WG3, and the optical beam will travel toward R4 and R5 through WG5, WG6. R4 and R5 cannot drop the optical waves from W5 or W6, so O1 and O0 will be active (See Fig. 9c). As a result, when $1.5I_0<I_{in}<2I_0$, the resulting code will be "11." Figure 10c shows that the normalized powers for both output ports are about 45%. In this case, the steady-state time is about 3.2 ps.

Figure 11 shows The output powers versus time for input optical pulses with the duration of 8 ps and intensities of (a) $0<I_{in}<0.5I_0$, (b) $0.5I_0<I_{in}<I_0$, (c) $I_0<I_{in}<1.5\ I_0$, and

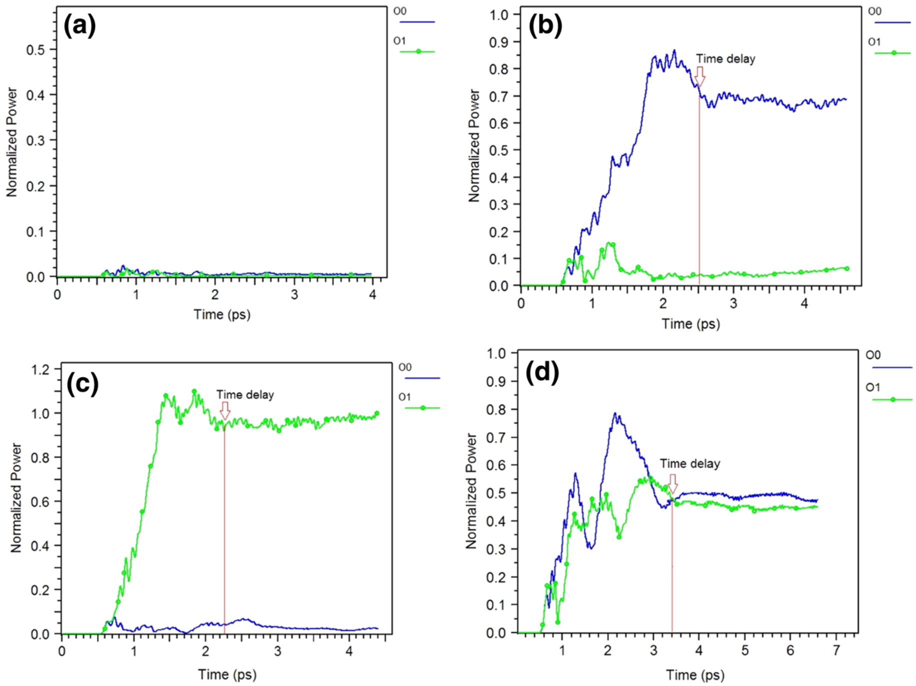

Fig. 10 The normalized power at the proposed OADC's output ports versus time for the optical intensities of **a** $0<I_{in}<0.5I_0$, **b** $0.5I_0<I_{in}<I_0$, **c** $I_0<I_{in}<1.5\ I_0$, and **d** $1.5\ I_0<I_{in}<2I_0$

(d) $1.5\ I_0<I_{in}<2I_0$. For the proposed OADC, the maximum rise and fall times are 2.5 ps and 1.5 ps, respectively (See Fig. 11c). Therefore, the sampling rate will be 125 GS/s for a two-bit ADC.

The working states of the proposed OADC are shown in Fig. 9 and listed in Table 1. Table 2 compares the results of the proposed structure with the results of articles published in recent years. The proposed structure's important advantages are high transmission power, low delay, low total loss consisting of leakage and waveguide losses, and the adjustability of every X-PCRR's resonance modes with the variations of the input optical power.

4 Conclusion

In summary, we proposed a new design of a two-bit optical OADC using five nonlinear X-PCRRs. This structure consisted of a three-channel demultiplexer followed by a two-bit binary encoder. Sampling and quantizing have been carried out by demultiplexer employing three X-PCRRs in which every X-PCRR consisted of linear and nonlinear dielectric rods. Two other X-PCRRs help optical encoder generates two-bit binary codes. The performance of the proposed OADC was numerically studied using the PWE and FDTD methods. The proposed structure has a maximum sampling rate of up to 125 GS/s, maximum time response of 4 ps, and a total footprint of 1785 μm^2. The proposed structure can easily be generalized to the OADC with greater accuracy, meaning more output bits.

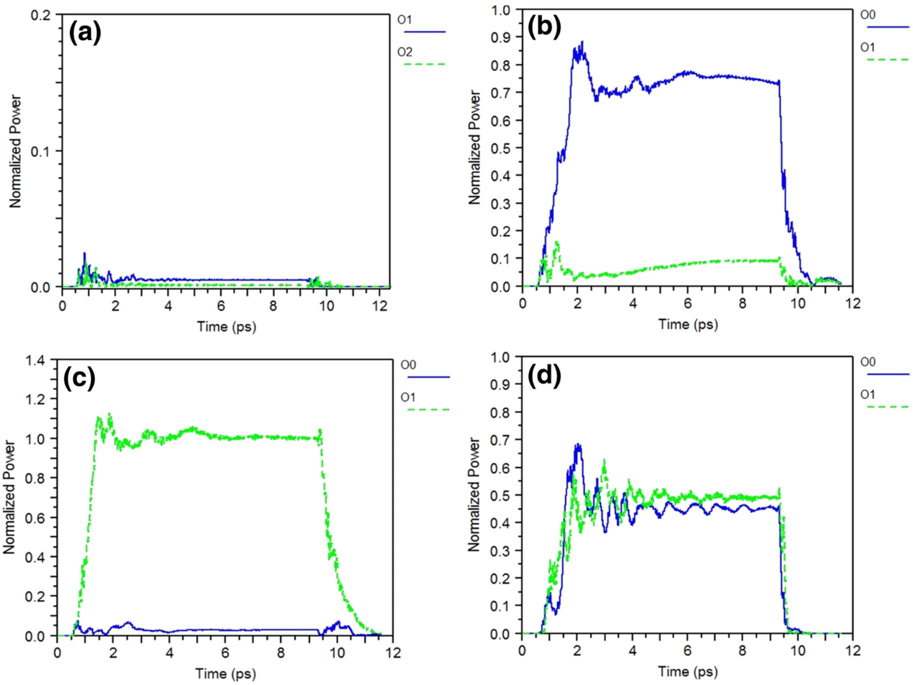

Fig. 11 The output powers versus time for input optical pulses with the duration of 8 ps and intensities of **a** $0 < I_{in} < 0.5I_0$, **b** $0.5I_0 < I_{in} < I_0$, **c** $I_0 < I_{in} < 1.5\ I_0$, and **d** $1.5\ I_0 < I_{in} < 2I_0$

Table 1 Working States of the Proposed OADC

Input intensity	Output (%)		Digital output states	
	O0	O1	O0	O1
$0 < I_{in} < 0.5I_0$	2	2	0	0
$0.5I_0 < I_{in} < I_0$	70	5	1	0
$I_0 < I_{in} < 1.5\ I_0$	2	95	0	1
$1.5\ I_0 < I_{in} < 2I_0$	45	45	1	1

Table 2 The comparison between the suggested structure and the structures in previous papers

Works	Sampling rate (GS/s)	Accuracy (bits)	Steady-state time	Footprint (μm^2)
Youssefi et al. (2012)	45	2	18.3	252
Mehdizadeh et al. (2017b)	52	2	14	924
Mehdizadeh et al. (2017c)	77	2	7.2	1520
Sani et al. (2020)	220	2	2.5	778
Xin and Linfeng (2020)	250	2	2	2016
This Work	125	2	4	1785

Declarations

Conflict of interest The authors declare that they have no known competing financial interests or personal relationships that could have appeared to influence the work reported in this paper.

References

Alden Mostaan, S.M., Saghaei, H.: A tunable broadband graphene-based metamaterial absorber in the far-infrared region. Opt. Quantum Electron. **53**, 96 (2021). https://doi.org/10.1007/s11082-021-02744-y

Alexoudi, T., Kanellos, G.T., Pleros, N.: Optical RAM and integrated optical memories: a survey. Light Sci. Appl. **9**, 1–16 (2020). https://doi.org/10.1038/s41377-020-0325-9

Aliee, M., Mozaffari, M.H., Saghaei, H.: Dispersion-flattened photonic quasicrystal optofluidic fiber for telecom C band operation. Photon. Nanostruct. Fundam. Appl. **40**, 100797 (2020). https://doi.org/10.1016/j.photonics.2020.100797

Alipour-Banaei, H., Jahanara, M., Mehdizadeh, F.: T-shaped channel drop filter based on photonic crystal ring resonator. Optik (Stuttg). **125**, 5348–5351 (2014)

Alipour-Banaei, H., Mehdizadeh, F., Serajmohammadi, S., Hassangholizadeh-Kashtiban, M.: A 2* 4 all optical decoder switch based on photonic crystal ring resonators. J. Mod. Opt. **62**, 430–434 (2015)

Andalib, P., Granpayeh, N.: All-optical ultracompact photonic crystal AND gate based on nonlinear ring resonators. J. Opt. Soc. Am. B. **26**, 10–16 (2009). https://doi.org/10.1364/josab.26.000010

Chen, Z., Li, Z., Li, B.: A 2-to-4 decoder switch in SiGe/Si multimode inteference. Opt. Express. **14**, 2671–2678 (2006). https://doi.org/10.1364/oe.14.002671

Danaee, E., Geravand, A., Danaie, M.: Wide-band low cross-talk photonic crystal waveguide intersections using self-collimation phenomenon. Opt. Commun. **431**, 216–228 (2019). https://doi.org/10.1016/j.optcom.2018.09.032

Danaie, M., Kaatuzian, H.: Bandwidth improvement for a photonic crystal optical Y-splitter. J. Opt. Soc. Korea. **15**, 283–288 (2011)

Diouf, M., Salem, A.B., Cherif, R., Saghaei, H., Wague, A.: Super-flat coherent supercontinuum source in As_388Se_612 chalcogenide photonic crystal fiber with all-normal dispersion engineering at a very low input energy. Appl. Opt. **56**, 163–169 (2017). https://doi.org/10.1364/ao.56.000163

Ebnali-Heidari, M., Saghaei, H., Koohi-Kamali, F., Naser-Moghadasi, M., Moravvej-Farshi, M.K.: Proposal for supercontinuum generation by optofluidic infiltrated photonic crystal fibers. IEEE J. Sel. Top. Quantum Electron. **20**, 582–589 (2014). https://doi.org/10.1109/JSTQE.2014.2307313

Fakouri-Farid, V., Andalib, A.: Design and simulation of an all optical photonic crystal-based comparator. Optik (Stuttg). **172**, 241–248 (2018). https://doi.org/10.1016/j.ijleo.2018.06.153

Fasihi, K.: All-optical analog-to-digital converters based on cascaded 3-dB power splitters in 2D photonic crystals. Optik (Stuttg). **125**, 6520–6523 (2014). https://doi.org/10.1016/j.ijleo.2014.08.030

Foroughifar, A., Saghaei, H., Veisi, E.: Design and analysis of a novel four-channel optical filter using ring resonators and line defects in photonic crystal microstructure. Opt. Quantum Electron. **53**, 101 (2021)

Ghanbari, A., Kashaninia, A., Sadr, A., Saghaei, H.: Supercontinuum generation for optical coherence tomography using magnesium fluoride photonic crystal fiber. Optik (Stuttg). **140**, 545–554 (2017). https://doi.org/10.1016/j.ijleo.2017.04.099

Ghanbari, A., Kashaninia, A., Sadr, A., Saghaei, H.: Opt. Quantum Electron. **50**, 411 (2018). https://doi.org/10.1007/s11082-018-1651-5

Gu, L., Jiang, W., Chen, X., Wang, L., Chen, R.T.: High speed silicon photonic crystal waveguide modulator for low voltage operation. Appl. Phys. Lett. **90**, 71105 (2007). https://doi.org/10.1063/1.2475580

Guo, Y., Zhang, S., Li, J., Li, S., Cheng, T.: A sensor-compatible polarization filter based on photonic crystal fiber with dual-open-ring channel by surface plasmon resonance. Optik (Stuttg) **193**, 162868 (2019). https://doi.org/10.1016/j.ijleo.2019.05.074

Hosseinzadeh Sani, M., Ghanbari, A., Saghaei, H.: An ultra-narrowband all-optical filter based on the resonant cavities in rod-based photonic crystal microstructure. Opt. Quantum Electron. **52**, 295 (2020a). https://doi.org/10.1007/s11082-020-02418-1

Hosseinzadeh Sani, M., Saghaei, H., Mehranpour, M.A., Asgariyan Tabrizi, A.: A novel all-optical sensor design based on a tunable resonant nanocavity in photonic crystal microstructure applicable in MEMS accelerometers. Photon. Sensors. (2020b). https://doi.org/10.1007/s13320-020-0607-0

Hussein, H.M.E., Ali, T.A., Rafat, N.H.: New designs of a complete set of photonic crystals logic gates. Opt. Commun. **411**, 175–181 (2018). https://doi.org/10.1016/j.optcom.2017.11.043

Jafari, D., Nurmohammadi, T., Asadi, M.J., Abbasian, K.: All-optical analog-to-digital converter based on Kerr effect in photonic crystal. Opt. Laser Technol. **101**, 138–143 (2018). https://doi.org/10.1016/j.optlastec.2017.11.007

Jile, H.: Realization of an all-optical comparator using beam interference inside photonic crystal waveguides. Appl. Opt. **59**, 3714–3719 (2020). https://doi.org/10.1364/ao.385744

Kaur, S.: Kaler RS (2014) 5 GHz all-optical binary counter employing SOA-MZIs and an optical NOT gate. J. Opt. **16**, 35201 (2014). https://doi.org/10.1088/2040-8978/16/3/035201

Kowsari, A., Saghaei, H.: Resonantly enhanced all-optical switching in microfibre Mach-Zehnder interferometers. Electron. Lett. **54**, 229–231 (2018). https://doi.org/10.1049/el.2017.4056

Kumar, R., Huybrechts, K., Liu, L., Spuessens, T., Roelkens, G., Geluk, E.J., Vries, T.D., Regreny, P., Thourhout, D.V., Baets, R., Morthier, G.: An ultra-small, low-power all-optical flip-flop memory on a silicon chip. Opt. InfoBase Conf. Pap. **4**, 182–187 (2010). https://doi.org/10.1038/nphoton.2009.268

Kuramochi, E., Nozaki, K., Shinya, A., Takeda, K., Sato, T., Matsuo, S., Taniyama, H., Sumikura, H., Notomi, M.: Large-scale integration of wavelength-addressable all-optical memories on a photonic crystal chip. Nat. Photon. **8**, 474–481 (2014). https://doi.org/10.1038/nphoton.2014.93

Martinez-Dorantes, M., Alt, W., Gallego, J., Ghosh, S., Ratschbacher, L., Völzke, Y., Meschede, D.: Fast nondestructive parallel readout of neutral atom registers in optical potentials. Phys. Rev. Lett. **119**, 180503 (2017). https://doi.org/10.1103/PhysRevLett.119.180503

Mehdizadeh, F., Alipour-Banaei, H., Serajmohammadi, S.: Study the role of non-linear resonant cavities in photonic crystal-based decoder switches. J. Mod. Opt. **64**, 1233–1239 (2017a). https://doi.org/10.1080/09500340.2016.1275854

Mehdizadeh, F., Soroosh, M., Alipour-Banaei, H., Farshidi, E.: All optical 2-bit analog to digital converter using photonic crystal based cavities. Opt. Quantum Electron. **49**, 38 (2017b). https://doi.org/10.1007/s11082-016-0880-8

Mehdizadeh, F., Soroosh, M.: A new proposal for eight-channel optical demultiplexer based on photonic crystal resonant cavities. Photonic Netw. Commun. **31**, 65–70 (2016). https://doi.org/10.1007/s11107-015-0531-1

Mehdizadeh, F., Soroosh, M., Alipour-Banaei, H., Farshidi, E.: Ultra-fast analog-to-digital converter based on a nonlinear triplexer and an optical coder with a photonic crystal structure. Appl. Opt. **56**, 1799–1806 (2017c). https://doi.org/10.1364/ao.56.001799

Miao, B., Chen, C., Sharkway, A., Shi, S., Prather, D.W.: Two bit optical analog-to-digital converter based on photonic crystals. Opt. Express. **14**, 7966–7973 (2006). https://doi.org/10.1364/oe.14.007966

Moniem, T.A.: All-optical digital 4 × 2 encoder based on 2D photonic crystal ring resonators. J. Mod. Opt. **63**, 735–741 (2016). https://doi.org/10.1080/09500340.2015.1094580

Monisha, S., Saranya, D., Rajesh, A.: Design and analysis of multi-hexagonal reversible encoder using photonic crystals. Opt. Quantum Electron. **51**, 6 (2018). https://doi.org/10.1007/s11082-018-1718-3

Moradi, M., Danaie, M., Orouji, A.A.: Design and analysis of an optical full-adder based on nonlinear photonic crystal ring resonators. Optik (Stuttg). **172**, 127–136 (2018)

Moradi, M., Danaie, M., Orouji, A.A.: Design of all-optical XOR and XNOR logic gates based on Fano resonance in plasmonic ring resonators. Opt. Quantum Electron. **51**, 154 (2019)

Moradi, R.: All optical half subtractor using photonic crystal based nonlinear ring resonators. Opt. Quantum Electron. **51**, 119 (2019). https://doi.org/10.1007/s11082-019-1831-y

Mostafa, T., El-Rabaie, E.-S.: Literature review on all-optical photonic crystal encoders and some novel trends. Menoufia J. Electron. Eng. Res. **28**, 153–184 (2019). https://doi.org/10.21608/mjeer.2019.62773

Naghizade, S., Khoshsima, H.: Low input power an all optical 4×2 encoder based on triangular lattice shape photonic crystal. J. Opt. Commun. **1**, 1–8 (2018). https://doi.org/10.1515/joc-2018-0019

Naghizade, S., Saghaei, H.: Tunable graphene-on-insulator band-stop filter at the mid-infrared region. Opt. Quantum Electron. **52**, 224 (2020a). https://doi.org/10.1007/s11082-020-02350-4

Naghizade, S., Saghaei, H.: A novel design of all-optical 4 to 2 encoder with multiple defects in silica-based photonic crystal fiber. Optik **222**, 165419 (2020b). https://doi.org/10.1016/j.ijleo.2020.165419

Nasirifar, R., Danaie, M., Dideban, A.: Dual channel optical fiber refractive index sensor based on surface plasmon resonance. Optik (Stuttg). **186**, 194–204 (2019)

Pahari, N., Guchhait, A.: All-optical serial data transfer between registers using optical non-linear materials. Optik (Stuttg). **123**, 462–466 (2012). https://doi.org/10.1016/j.ijleo.2011.05.006

Parandin, F.: High contrast ratio all-optical 4 × 2 encoder based on two-dimensional photonic crystals. Opt. Laser Technol. **113**, 447–452 (2019). https://doi.org/10.1016/j.optlastec.2019.01.003

Parandin, F., Karkhanehchi, M.M., Naseri, M., Zahedi, A.: Design of a high bitrate optical decoder based on photonic crystals. J. Comput. Electron. **17**, 830–836 (2018). https://doi.org/10.1007/s10825-018-1147-3

Poustie, A., Manning, R.J., Kelly, A.E., Blow, K.J.: All-optical binary counter. Opt. Express. **6**, 69–74 (2000). https://doi.org/10.1364/oe.6.000069

Raei, R., Ebnali-Heidari, M., Saghaei, H.: Supercontinuum generation in organic liquid–liquid core-cladding photonic crystal fiber in visible and near-infrared regions. J. Opt. Soc. Am. B. **35**, 323–330 (2018). https://doi.org/10.1364/JOSAB.35.000323

Rahmani, A., Mehdizadeh, F.: Application of nonlinear PhCRRs in realizing all optical half-adder. Opt. Quantum Electron. **50**, 30 (2018). https://doi.org/10.1007/s11082-017-1301-3

Rajasekar, R., Thavasi Raja, G., Jayabarathan, J.K., Robinson, S.: High speed nano-optical encoder using photonic crystal ring resonator. Photonic Netw. Commun. **40**, 31–39 (2020). https://doi.org/10.1007/s11107-020-00891-y

Rakhshani, M.R., Mansouri-Birjandi, M.A.: Realization of tunable optical filter by photonic crystal ring resonators. Optik (Stuttg). **124**, 5377–5380 (2013). https://doi.org/10.1016/j.ijleo.2013.03.114

Saghaei, H.: Supercontinuum source for dense wavelength division multiplexing in square photonic crystal fiber via fluidic infiltration approach. Radioengineering. **26**, 16–22 (2017). https://doi.org/10.13164/re.2017.0016

Saghaei, H.: Dispersion-engineered microstructured optical fiber for mid-infrared supercontinuum generation. Appl. Opt. **57**, 5591–5598 (2018). https://doi.org/10.1364/ao.57.005591

Saghaei, H., Ebnali-Heidari, M., Moravvej-Farshi, M.K.: Midinfrared supercontinuum generation via As_2Se_3 chalcogenide photonic crystal fibers. Appl. Opt. **54**, 2072–2079 (2015). https://doi.org/10.1364/ao.54.002072

Saghaei, H., Elyasi, P., Karimzadeh, R.: Design, fabrication, and characterization of Mach-Zehnder interferometers. Photon. Nanostruct. Fundam. Appl. **37**, 100733 (2019). https://doi.org/10.1016/j.photonics.2019.100733

Saghaei, H., Ghanbari, A.: White light generation using photonic crystal fiber with sub-micron circular lattice. J. Electr. Eng. **68**, 282–289 (2017). https://doi.org/10.1515/jee-2017-0040

Saghaei, H., Heidari, V., Ebnali-Heidari, M., Yazdani, M.R.: A systematic study of linear and nonlinear properties of photonic crystal fibers. Optik (Stuttg). **127**, 11938–11947 (2016a). https://doi.org/10.1016/j.ijleo.2016.09.111

Saghaei, H., Moravvej-Farshi, M.K., Ebnali-Heidari, M., Moghadasi, M.N.: Ultra-wide mid-infrared supercontinuum generation in as40se60 chalcogenide fibers: solid core PCF versus SIF. IEEE J. Sel. Top. Quantum Electron. **22**, 279–286 (2016b). https://doi.org/10.1109/JSTQE.2015.2477048

Saghaei, H., Seyfe, B.: New approach to closed-loop power control in cellular CDMA systems under multipath fading. In: 2008 International Conference on Wireless Communications, Networking and Mobile Computing, WiCOM 2008 (2008)

Saghaei, H., Seyfe, B., Bakhshi, H., Bayat, R.: Novel approach to adjust the step size for closed-loop power control in wireless cellular code division multiple access systems under flat fading. IET Commun. **5**, 1469–1483 (2011). https://doi.org/10.1049/iet-com.2010.0029

Saghaei, H., Van, V.: Broadband mid-infrared supercontinuum generation in dispersion-engineered silicon-on-insulator waveguide. J. Opt. Soc. Am. B. **36**, A193–A202 (2019). https://doi.org/10.1364/josab.36.00a193

Saghaei, H., Zahedi, A., Karimzadeh, R., Parandin, F.: Line defects on photonic crystals for the design of all-optical power splitters and digital logic gates. Superlattices Microstruct. **110**, 133–138 (2017). https://doi.org/10.1016/j.spmi.2017.08.052

Sani, M.H., Khosroabadi, S., Shokouhmand, A.: A novel design for 2-bit optical analog to digital (A/D) converter based on nonlinear ring resonators in the photonic crystal structure. Opt. Commun. **458**, 124760 (2020). https://doi.org/10.1016/j.optcom.2019.124760

Sethi, P., Roy, S.: Ultrafast all-optical flip-flops, simultaneous comparator-decoder and reconfigurable logic unit with silicon microring resonator switches. IEEE J. Sel. Top. Quantum Electron. **20**, 118–125 (2014). https://doi.org/10.1109/JSTQE.2013.2295179

Sharifi, H., Hamidi, S.M., Navi, K.: A new design procedure for all-optical photonic crystal logic gates and functions based on threshold logic. Opt. Commun. **370**, 231–238 (2016)

Sinha, R.K., Rawal, S.: Modeling and design of 2D photonic crystal based Y type dual band wavelength demultiplexer. Opt. quantum Electron. **40**, 603–613 (2008)

Tabrizi, A.A., Saghaei, H., Mehranpour, M.A., Jahangiri, M.: Enhancement of absorption and effectiveness of a perovskite thin-film solar cell embedded with Gold nanospheres. Plasmonics (2021). https://doi.org/10.1007/s11468-020-01341-1

Talebzadeh, R., Soroosh, M., Kavian, Y.S., Mehdizadeh, F.: Eight-channel all-optical demultiplexer based on photonic crystal resonant cavities. Optik (Stuttg). **140**, 331–337 (2017). https://doi.org/10.1016/j.ijleo.2017.04.075

Tavakoli, F., Zarrabi, F.B., Saghaei, H.: Modeling and analysis of high-sensitivity refractive index sensors based on plasmonic absorbers with Fano response in the near-infrared spectral region. Appl. Opt. **58**, 5404–5414 (2019). https://doi.org/10.1364/AO.58.005404
Tavousi, A., Mansouri-Birjandi, M.A.: Optical-analog-to-digital conversion based on successive-like approximations in octagonal-shape photonic crystal ring resonators. Superlattices Microstruct. **114**, 23–31 (2018). https://doi.org/10.1016/j.spmi.2017.11.021
Uda, T., Ishii, A., Kato, Y.K.: Single carbon nanotubes as ultrasmall all-optical memories. ACS Photonics. **5**, 559–565 (2018). https://doi.org/10.1021/acsphotonics.7b01104
Wen, K., Yan, L., Pan, W., Luo, B., Guo, Z., Guo, Y.: Wavelength demultiplexing structure based on a plasmonic metal-insulator-metal waveguide. J. Opt. **14**, 75001 (2012). https://doi.org/10.1088/2040-8978/14/7/075001
Xin, G., Linfeng, Z.: All-optical analog to digital converter based on nonlinear photonic crystal ring resonators. Photonics Nanostructures Fundamentals Appl **41**, 100817 (2020). https://doi.org/10.1016/j.photonics.2020.100817
Yang, Y.-P., Lin, K.-C., Yang, I.-C., Lee, K.-Y., Lee, W.-Y., Tsai, Y.-T.: All-optical photonic-crystal encoder capable of operating at multiple wavelengths. Optik (Stuttg). **142**, 354–359 (2017). https://doi.org/10.1016/j.ijleo.2017.05.067
Younis, R.M., Areed, N.F.F., Obayya, S.S.A.: Fully integrated and and or optical logic gates. IEEE Photonics Technol. Lett. **26**, 1900–1903 (2014). https://doi.org/10.1109/LPT.2014.2340435
Youssefi, B., Moravvej-Farshi, M.K., Granpayeh, N.: Two bit all-optical analog-to-digital converter based on nonlinear Kerr effect in 2D photonic crystals. Opt. Commun. **285**, 3228–3233 (2012). https://doi.org/10.1016/j.optcom.2012.02.081